

In-Wheel Motor for a Small Hybrid Electric Vehicle: Design, Realization and Experimental Characterization

Christophe Espanet, Member, IEEE
Frédéric Dubas, Hoang Minh Mã, Didier Chamagne
FEMTO-ST Institute, ENERGY Department
University of Franche-Comte
Belfort, France
christophe.espanet@univ-fcomte.fr

Robert Bernard, Pascal Bigot

Novelte Systeme
Belfort, France

robert.bernard@novelte-systeme.fr

Abstract – This paper presents a surface mounted (SM) permanent-magnet (PM) in-wheel motor for the propulsion of a small plug-in hybrid electric vehicle (PHEV) for urban use. The electric machine is a fractional number of slots per number of poles motor using concentrated winding (wound around one tooth). First the authors detail the technical specifications: the maximal torque and power respectively equal to 240 N.m and 4.5 kW. Then they justify briefly the choice of the motor type and they present the optimal design and the mechanical analysis (vibrations). Finally, the realization of the motor is described (i.e., the stator laminations, the stator concentric windings, the external rotor structure...) and the experimental tests are presented to highlight the real performances of the in-wheel motor.

Keywords – In-wheel motor, PM machines, Plug-in hybrid electric vehicles, High torque density

I. INTRODUCTION: PHEBUS, A SMALL PLUG-IN HYBRID ELECTRIC VEHICLE FOR URBAN USE

In this paper, the authors consider the motorization of a small PHEV for urban use, which is called PHEBUS. The architecture of the studied PHEV is presented in Figure 1. It is based on a small diesel vehicle (see Figure 2). The PHEV is obtained by adding two electrical in-wheel motors integrated in the two rear wheels and by downsizing the existing internal combustion engine (ICE) used to drive the front wheels. The vehicle uses a battery (230 V) and ultra-capacitors (UC) as supply power [1]. This PHEV may work in two main modes: the electric mode or the hybrid mode. The electric mode is used in downtown to avoid gas emissions. The hybrid mode is used out of the town to keep an acceptable autonomy. Since the ICE is downsized, the gas emissions are also reduced, and the two in-wheel motors can be used in addition of the ICE, to recover the power available with the initial ICE (boost function). Moreover, the electric motors can also be used as generators during braking or when the road slope is negative. They will convert kinetic energy of the vehicle into electric energy, that will used to recharge the UC in priority, or the battery when the UC are

completely charged. Then, as for the recharge, the electric energy of the UC is used in priority. Finally, this energy management and the PHEV structure leads to a reduction of the energy consumption and of gas emissions, with a really simple hybrid architecture. But this solution needs the design of two special electric motors integrated in the rear wheels and providing a high torque in case of direct drive. This is the aim of the work presented in this paper.

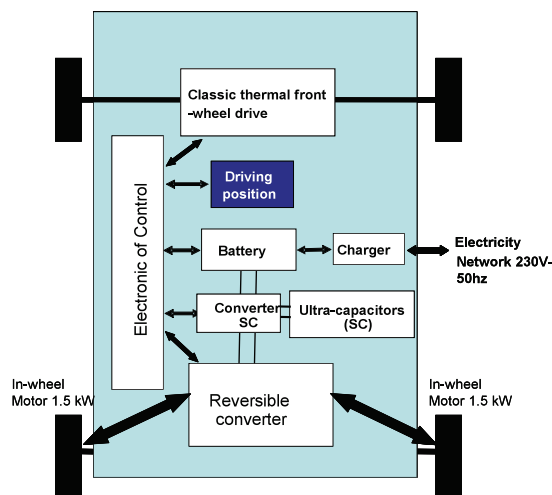


Figure 1 Structure of the studied hybrid vehicle



Figure 2 PHEBUS vehicle (AIXAM-MEGA company)

II. TECHNICAL SPECIFICATIONS OF THE IN-WHEEL MOTORS

In this section, the technical specifications of the in-wheel motor are described. Firstly the motor is submitted to geometrical constraints. Since the motor is integrated in a standard 15'' wheel, the overall dimensions are constrained: the outer diameter R_{ext} and the machine length L_{mach} have to be respectively lower than 155 mm and 200 mm. In order not to damage the comfort and the security or not to modify strongly the suspension system, the wheel weight increase has to be limited, so that the active parts weight of one machine should be lower than 10kg.

An important choice concerns the use or not of a reduction gear. It is clear that the use of a reduction gear enables a reduction of the torque that the motor has to provide and an increase of the rotational speed in the same time. As it is well known that the volume of an electric machine is directly linked to its maximal torque, the use of reduction gear enables a reduction of the volume, weight and cost of the motor. But, on the other hand, the gear will create additional losses and noise, it has its own weight and it will need maintenance. Moreover, the integration of the reduction gear in the wheel is not an easy task, especially for small vehicles and wheels. Then, if the use of a gear is preferable for large vehicle, it could be a drawback for small vehicle such as bicycle, scooter or quadricycle. That's why, for the PHEV considered in this paper, it has been chosen to realize the in-wheel motor with a direct drive, in particular to make possible the integration in the wheel of the motor and the foundation brake drum.

Then, the next constraints refer to the torque and the power that the motor has to be able to produce for a given vehicle speed. To obtain actual values, the real vehicle has been simulated with using special software dedicated to the simulation of the vehicle dynamics. With such a software, it is possible to simulate all the missions imposed by the vehicle specifications: maximal acceleration, hill start, on rise of sidewalk, electric braking... And the results enable to check the vehicle handling, to design the suspension of the back axle and to define the constraints of torque, rotational speed and power of the in-wheel motors. By using this approach, it has been shown that only 6 particular working points can be used to design the motors. Those points are deduced from the missions' simulations and they are summarized by the torque and power characteristics presented in Figure 3. More precisely, the working point 1 represents the maximal torque that each of the two rear wheels has to provide to climb a slopping road of 16 % with the maximal load. The working point 3 represents the maximal power obtained for acceleration at medium vehicle speed (around 25 km/h). The point 4 is called rated point since it corresponds to the quadratic mean value of the torque and speed over a representative working that has been defined with the experience of the vehicle manufacturer. The point 5 corresponds to the maximal speed of the vehicle in electric mode (50 km/h). Finally, the point 6 corresponds to the maximal speed in thermal mode (65 km/h): at this speed,

the line voltage of the motor has to be controlled in order to avoid a conduction of the inverter diodes. Moreover, at this particular point, the motor total losses (copper, iron and PM) have to be limited in order not to damage the energy consumption. A maximal value of 150 W for each motor losses is targeted.

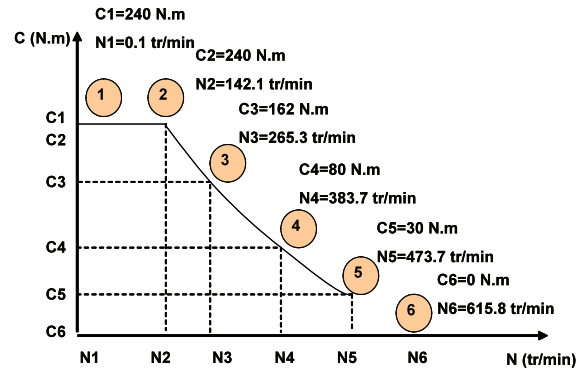
The last constraints refer to the thermal behavior. To avoid complex cooling system, it has been decided to design a motor with natural cooling. The working points 1 and 2 have to be reached during at least 15 s and the point 3 during at least 15 min.

III. DESIGN OF THE MOTOR

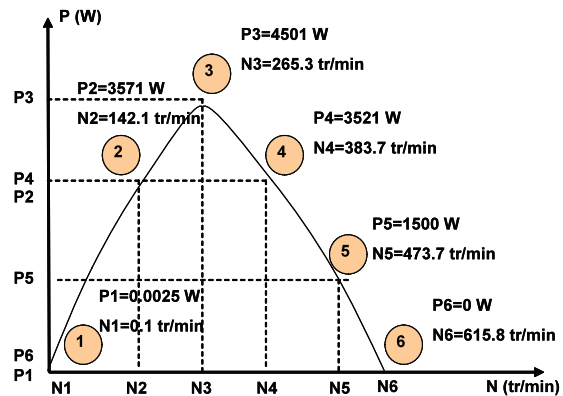
In this section, the authors present first a short review of existing in-wheel motors and vehicles with those motors. Then they describe the different steps of the motor design for the PHEV considered here.

A. Brief state of the art

In this paragraph, a short and non-exhaustive review of existing in-wheel motors is presented. The aim is to detail some realizations (for different types of vehicles) and also to determine the current choices of technology (motor type and architecture).



(a) Torque/rotating speed characteristic



(a) Power/rotating speed characteristic

Figure 3 Mechanical characteristics of the in-wheel motors

The first example is rather anecdotic. It deals with an old hybrid electric vehicle presented for the first time at the Universal Exhibition in Paris, in 1898, and developed by Porsche (see Figure 4). The vehicle uses 4 in-wheel motors and an ICE. This example proves that the idea of hybrid electric vehicle with in-wheel motors is not really new!

The second example deals with the motor developed in 2005 by Wavcrest Laboratories initially for the US Army [2]. Then, this in-wheel motor was used in powerful electric bicycles (see Figure 5). The motor is a PM synchronous motor with concentric windings. It is located in the bicycle wheel without reduction gear. The power equals to 750-1000 W and the maximal torque equals to 80 N.m; the motor is fed by a DC voltage (36 V) and a voltage source inverter; the cooling is natural.

The third example deals with in-wheel motors from TM4 Company [3]. This latter is historic on the in-wheel-motor market. It comes from the researches achieved by the Pierre Couture (Hydro-Quebec) during the 80s. Now TM4 develop not only in-wheel motors but also several machines for EV and HEV, generators for renewable energy and other PM electric machines for different applications. The initial topology was a SMPM synchronous machine with external motor and without reduction gear. Now the in-wheel motor is rather a hub-motor (see Figure 6) instead of a rim-motor. In the example of the C-Métisse (see Figure 6), the motor performances are the following:

- Continuous power: 15 kW;
- Maximal torque: 300 N.m;
- Maximal rotating speed: 1900 rpm;
- Fluid cooling.

The rotor is external to maximize the air-gap diameter and thus the specific torque. The PMs are surface mounted with an optimized shape to minimize the detent torque.

The fourth example deals with the in-wheel motors from Magnet Motors [4], which is another major company on the market of in-wheel motors. The topology is close to the one used by TM4: surface mounted PM and external rotor. But Magnet Motors uses a concentric winding, instead of an overlapped one for TM4. Two examples of motors are presented in TABLE I.

The fifth example deals with the concept of electric wheel from the Company Michelin. Contrary to the previous example, this in-wheel motor uses a reduction gear. As it can be shown in Figure 7a, the idea of the concept is to integrate the whole functions of a vehicle drive: an electric motor, an electrical active suspension and a reduction gear. The ratio is not public, but, according to the performances of existing vehicle, the value is around 10, which it is really challenging regarding the mechanical resistance. The use of the gear enables a high energy conversion frequency, so that it is possible to reduce the volume of the motor (around 30kW for a volume of around 6 liters). The motor technology is presented in Figure 7b (stator with concentric windings) and Figure 7c (rotor with embedded PMs) [5]. Finally, an example of sport vehicle is presented in Figure 7d.

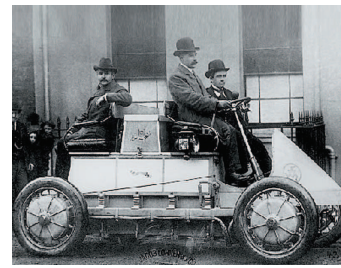


Figure 4 In-wheel motor of the HEV Lohner-Porsche, 1898



Figure 5 Wavcrest Laboratories in-wheel motor and an application to a bicycle, 2005

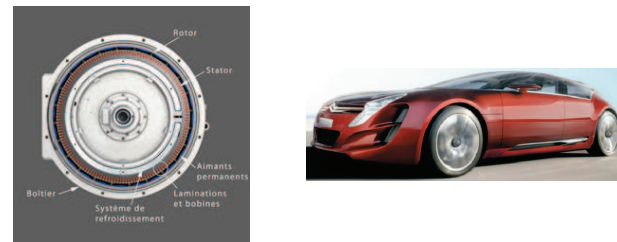
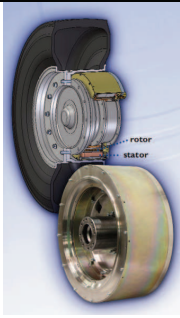
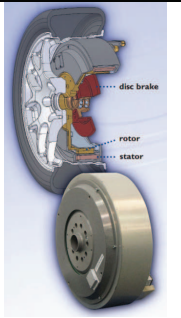
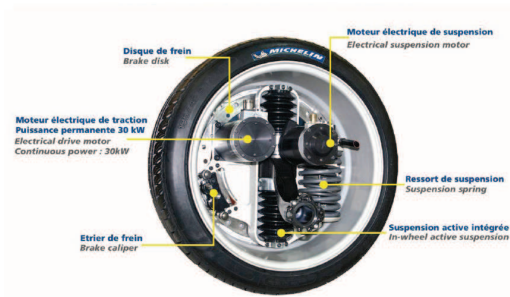


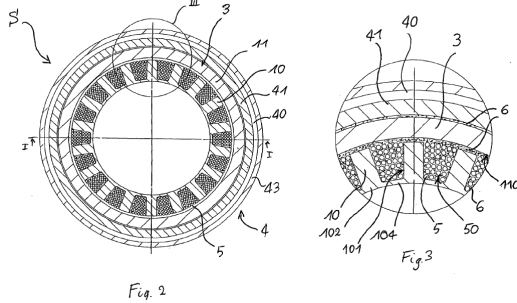
Figure 6 In-wheel motor of TM4 and application to the HEV C-Metisse, 2006

TABLE I EXAMPLE OF MAGNET MOTORS IN-WHEEL MOTORS

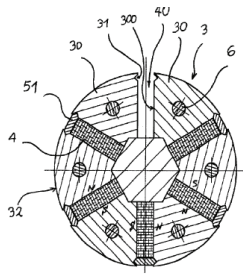
| Characteristic | Motor M69 | Motor M70 |
|------------------------------|---|---|
| Illustration |  |  |
| Continuous power (kW) | 120 | 50 |
| Maximal torque (N.m) | 2130 | 1050 |
| Maximal rotating speed (rpm) | 3210 | 2200 |
| Sizes | Ø 478mm x 180 mm | Ø 437mm x 134 mm |
| In-wheel motor weight (kg) | 90 | 34 |
| Cooling type | Fluid | Fluid |



(a) Electric wheel of Michelin: concept



(b) Electric wheel of Michelin: stator



(c) Electric wheel of Michelin: rotor



(d) Venturi Volage: EV with electric wheel of Michelin

Figure 7 The electric wheel from Michelin: concept, topology and application to the Venturi Volage

| | Units | PD18 |
|----------------------------------|-------|-----------|
| Peak output power @400Vdc | kW | 81 |
| Continuous output power @ 400Vdc | kW | 64 |
| Peak output torque | Nm | 800 |
| Continuous output torque | Nm | 500 |
| Nominal input voltage range | Vdc | 200 – 400 |
| Width | mm | 115 |
| Diameter | mm | 420 |
| Total motor mass | kg | 31 |

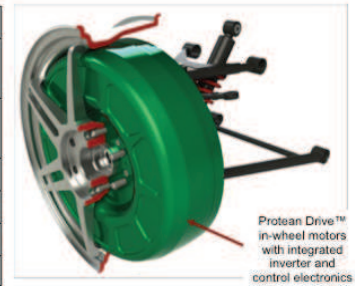


Figure 8 Protean Drive in-wheel motor

The last example deals with the in-wheel motor from Protean Drive Company [6]. The technical characteristics and an illustration are presented in Figure 8. The main originality of this machine is the integration of the power electronic in the machine.

B. Choice of the motor type

The first step of the design is to define the motor type. As a conclusion of the previous paragraph, even if the analysis is not exhaustive, it can be observed that most in-wheel motors use direct drive, PMs, external rotors and concentric windings. Indeed, in order to reach a high torque density (240 Nm with a weight lower than 10 kg) without reduction gear, the use of PM synchronous machine (PMSM) with high energy PM seems to be the best choice. For a rather discoid geometry (diameter = 1.5 x length), axial flux machine could be a good solution, but for an in-wheel motor, the mechanical resistance is a strong constraint. For example, the motor needs to be safe after an impact against a sidewalk at a speed of 20 km/h; this is really difficult with an axial flux machine and the risk of “bonding” between the rotor and the stator is high. Then, the authors have chosen the most obvious topology with an external rotor and surface mounted PMSM (SMPMSM). This structure has the advantage to be really easily integrated in a wheel, since the rim can be mounted directly of the rotor. Moreover the use of an external rotor enables to obtain a high air-gap diameter, increasing the torque. However, the tow main drawbacks are the following: (1) with surface mounted PM motors, flux weakening is not easy and it could lead to an over-sizing of the power electronic; (2) the bell-shaped geometry of the rotor could lead to amplify acoustic noise in case of rotor vibration.

In [7], the authors have compared two windings for this application: a diametric winding with one slot per pole and phase and a concentric winding verifying $N_d = 2p \pm 2$ [8]. Even if the winding coefficient is the highest with the first one, the second winding is preferred for the following reasons. Firstly, the concentric windings can be easily automated, so that its cost is reduced. Secondly, the depth of the end-winding is smaller, thus for a given length of machine, the active part length can be increased and the torque too, leading finally to a high torque per unit of copper

losses. Thirdly, the choice of $N_d = 2p \pm 2$ enables a rather sinusoidal back EMF. And lastly, the slot leakages are higher, so that the cyclic inductance is higher and consequently it improves the moderate capacity of flux weakening of SMPMSM. However, the stator MMF of motors with concentric winding where $N_d = 2p \pm 2$ have high sub-harmonics, leading possibly to strong PM losses [9] and vibrations. After a first analytical optimal design (see paragraph C), these two points have been carefully studied with 2D finite-elements method (FEM) simulations (see paragraph D).

C. Optimal design

Once the motor type has been chosen, the second step of the design deals with an optimal design using a multi-physics analytical model and following the approach already described in [10] and [11]. The analytical model is rather classical and it includes structural equations, magnetic equations, electro-mechanic equations and thermal equations. The analytical equation is quite large and it contains around 80 equations for each working point (working equations are rewritten for each point). The structural equations deal with the various relationships between all the geometrical parameters and the expressions of active parts volumes and weight (stator laminations, windings, rotor yoke and PMs). The magnetic equations are classically computed by solving the Maxwell's equations in the air-gap and the PMs using the variable separation [12]. The flux densities in the different parts of the machine are then deduced by applying the flux conservation law and the electromagnetic torque is computed using the Maxwell stress tensor. The electro-mechanic equations are formalized with an equivalent single-phase electric diagram, including the resistance of one phase, the cyclic inductance ($L_d = L_q$ with SMPMSM), the back EMF and an equivalent resistance modeling the stator and the PM iron losses. Finally, the thermal equations are relatively simple. For the maximal torque working, an adiabatic behavior is considered in order to limit the heating of the copper. And, for the other points, total losses have been constrained, using previous experience with comparable machines. However, the limit of losses has been validated with 3D FEM steady state thermal simulations after the analytical design.

With using the software Pro@Design, it was possible to optimize the motor. The input of the software is the analytical model and the output is a program that uses the model and also a SQP algorithm, enabling to optimize the machine, in respect with the different constraints of design (defined previously in the technical specifications). In our case, we have optimized the total weight of the motor and it has been possible to reach a total weight of 8 kg. Besides, the PM weight equals to 0.9 kg and the efficiency of the rated point equals to 92%. The machine has 28 poles and 30 teeth. The main technical characteristics are presented in TABLE II.

TABLE II TECHNICAL CHARACTERISTICS OF THE THEORETICAL PHEBUS IN-WHEEL MOTOR

| Characteristic | Numerical value |
|--------------------------------|-----------------|
| Maximal power (kW) | 4.5 |
| Maximal speed (rpm) | 620 |
| Torque at maximal load (N.m) | 162 |
| Peak torque during (N.m) | 240 |
| Efficiency at maximal load (%) | 92 |
| Global weight (kg) | 8 |
| Magnets' weight (kg) | 0.9 |
| Number of pole pairs | 14 |
| Air-gap (mm) | 2 |
| Air-gap flux density (T) | 0.85 |
| Resistance (mΩ) | 472 |
| Inductance (mH) | 4,13 |
| Back EMF coefficient (Wb) | 2,56 |

D. Mechanical analysis

As it has been explained in the section III.B, one strong constraint with fractional winding machines deals with the vibrations. In the present case, it is all the most critical that the rotor has a bell-shaped geometry. Then we have carefully studied the mechanical behavior of the rotor [13]. In a first step, we have done a nodal analysis of the rotor. Then, knowing the rotating speed range, we have analyzed the risks of resonance, i.e. the possibility that forces variations applied to the rotor excite a mode of vibration.

To achieve that, the forces distribution on the rotor has been calculated with 2D FEM electromagnetic simulations. Then, those forces have been applied to a 3D mechanical model to calculate deformation for each possible mode of vibration. The Figure 9 summarizes and illustrates the different steps of this calculation, for the worst case (risk of excitation of mode 2 with a rotating speed of 474 rpm). The observed deformations are lower than 30 μm, so that the risks of mechanical problem or acoustic noise are limited.

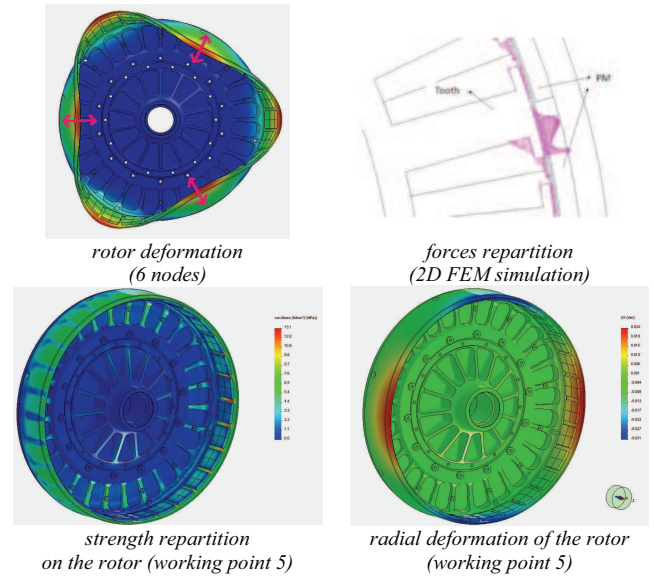


Figure 9 Mechanical study of the in-wheel motor at the working point 5

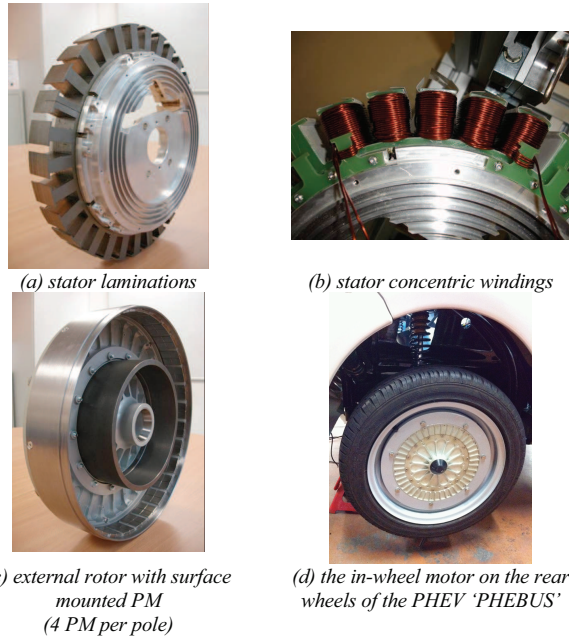


Figure 10 The different parts of the realized in-wheel motor

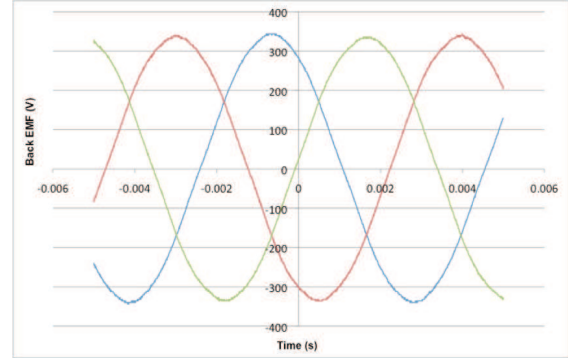
IV. REALIZATION OF THE MOTOR

In this section, we present the different active parts of the realized machine. Figure 10.a & b describes the stator laminations and the concentric windings. The rotor structure with the segmentation of PMs (axial and circumferential) is shown in Figure 10.c. It can be seen that the poles are segmented in 4 pieces to limit the eddy currents circulation and the corresponding PM losses. Finally, Figure 10.d shows the complete in-wheel motor placed in the vehicle.

V. EXPERIMENTAL CHARACTERIZATION

This last section presents the main results of the in-wheel motor experimental characterization. They are summarized in the Figure 11. Figure 11.a presents the chronogram of the back EMF at 617 rpm; the magnitude of 235 V can be compared with the magnitude calculated with the analytical model, which equals to 238 V. Figure 11.b presents the eddy-current PM losses measurements for different rotating speed. These losses have been obtained with three measurements. The first one uses a rotor without PM, leading to measure the friction losses. The second measurement uses a rotor with segmented poles (4 pieces) and the last one uses a rotor without segmentation. If we assume that the eddy-current PM losses are strongly reduced with segmented poles and that it can be neglected in comparison with iron losses, it is possible to determine the iron losses and the eddy-current PM losses. The good agreement between measurements and calculations enables the validation of the calculation model. However the segmented rotor will be used in the final motor (see Figure 10.c). Figure 11.c presents the static torque for a given value of the current magnitude. The static torque is obtained with a fixed rotor and by feeding the stator phases with current à very low frequency to create a low speed rotating field. It is

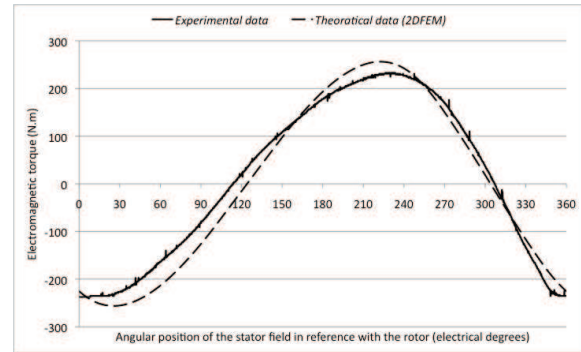
interesting in the sense that the maximum value of this curve gives the torque that can be obtained for a given current value. Figure 11.d gives the evolution of this maximal value with current magnitude for two real motors and for the theoretical calculation. The results of Figure 11.c & d validate the calculation. Figure 11.e gives the evolution of the motor efficiency for different working points. It shows that the efficiency is always higher than 85 % and even higher than 90 % for a large part of the considered working points. Finally, Figure 11.f present thermal measurements obtained for maximal torque working. It shows that the maximal torque can be applied during 30 seconds with a maximal heating of 50°C (obtained in the end-windings). This result is satisfying regarding the motor specifications.



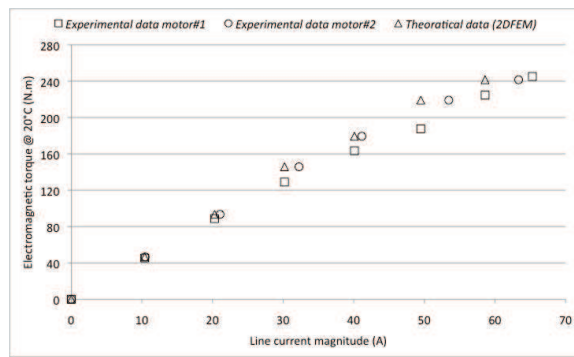
(a) Chronogram of back EMF ($N = 617 \text{ rpm}$, $T = 25^\circ\text{C}$)

| Working point | PM temperature ($^\circ\text{C}$) | Rotating speed (rpm) | PM losses (model) | PM losses (measurements) |
|---------------|-------------------------------------|----------------------|-------------------|--------------------------|
| 2 | 50°C | 140 | 2,6 | 2,0 |
| 3 | 50°C | 265,3 | 9,4 | 8,0 |
| 4 | 50°C | 383,7 | 19,6 | 7,5 |
| 5 | 50°C | 473,7 | 29,7 | 24,5 |
| 6 | 50°C | 615,8 | 50,1 | 42,5 |

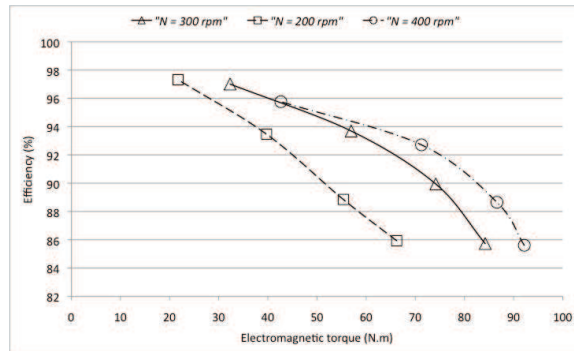
(b) Analysis of PM losses (rotor without segmentation)



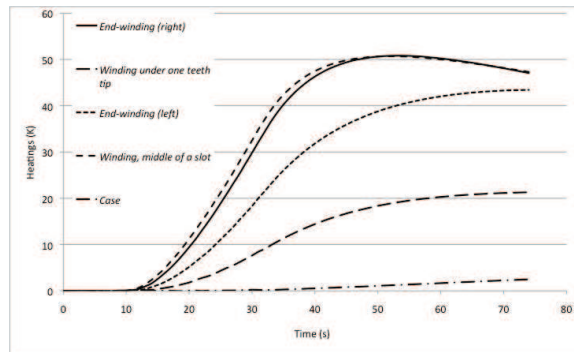
(c) Static torque (at maximal current magnitude $I_{\text{max}} = 66 \text{ A}$)



(d) Evolution of the static torque versus the current magnitude



(e) Evolution of the efficiency with torque for different rotating speeds



(f) Heating at maximal torque (240 N.m)

Figure 11 Experimental results of the in-wheel motor characterization

VI. CONCLUSIONS

In this paper, the authors have presented the design of an in-wheel motor that will drive a small PHEV. The technical specifications and the design have been briefly described. The motor has to provide a maximal torque of 240 Nm in a

volume lower than 15 l with natural cooling. The maximal power equals to 4.5 kW. By using optimization a motor of 12 kg has been designed (8 kg of active parts). It is a surface mounted PM synchronous motor with external rotor. Particular attention has been paid with vibrations and the authors have checked that the working is safe with FEM mechanical simulations. Finally the authors have presented experimental results, which on the one hand validate the calculation model, and on the other hand validate the obtaining of targeted performances. To summarize the performances, the obtained direct drive motor has a specific maximal torque of 30 Nm/kg (active parts) and presents an efficiency of more than 90 % for maximal power working.

REFERENCES

- [1] Loukakou, D.; Gualous, H.; Cheng Y.; Espanet, C.; Dubas, F.; "Sizing and experimental characterization of ultra-capacitors for small urban hybrid electric vehicle," Vehicle Power and Propulsion Conference, IEEE-VPPC'10, pp.01-07, 01-03 Sept. 2010, Lille, France.
- [2] <http://www.wavecrestlabs.com/>
- [3] <http://www.tm4.com/>
- [4] www.magnet-motor.com/
- [5] Michelin patents about its concept of electric-wheel: FR2898836A1A1, EP1901416A2, EP1359657A1, WO0235685A1, EP1756929A1
- [6] <http://www.proteanelectric.com/>
- [7] Mai, H.C.M.; Dubas, F.; Chamagne, D.; Espanet, C.; "Optimal design of a surface mounted permanent magnet in-wheel motor for an urban hybrid vehicle," Vehicle Power and Propulsion Conference, IEEE-VPPC'09, pp.481-485, 7-10 Sept. 2009, Dearborn, USA.
- [8] Cros, J.; Viarouge, P.; "Synthesis of high performance PM motors with concentrated windings," IEEE Transactions on Energy Conversion, vol.17, no.2, pp.248-253, June 2002.
- [9] Bianchi, N.; Bolognani, S.; Fornasiero, E.; "An Overview of Rotor Losses Determination in Three-Phase Fractional-Slot PM Machines," IEEE Transactions on Industry Applications, vol.46, no.6, pp.2338-2345, Nov.-Dec. 2010
- [10] Espanet, C.; Kauffmann, J.M.; Wurtz, F.; Bigeon, J.; "Application of a new optimization approach to the design of electrical wheels," IEEE Transactions on Energy Conversion, vol.14, no.4, pp.952-958, Dec 1999
- [11] Espanet, C.; Miraoui, A.; Kauffmann, J.-M.; "Optimal design of an high torque DC brushless in-wheel motor," IEEE International Electric Machines and Drives Conference, IEMDC'03, vol.3, pp. 1402-1409, 1-4 June 2003, Madison, USA.
- [12] Zhu, Z.Q.; Howe, D.; Bolte, E.; Ackermann, B.; "Instantaneous magnetic field distribution in brushless permanent magnet DC motors. I. Open-circuit field," IEEE Transactions on Magnetic, vol.29, no.1, pp.124-135, Jan 1993.
- [13] Mai, H.C.M.; Bernard, R.; Bigot, P.; Dubas, F.; Chamagne, D.; Espanet, C.; "Consideration of Radial Magnetic Forces in Brushless DC Motors," IEEE-ICEMS'10, pp.998-1003, 10-13 Oct. 2010, Incheon, Korea.